PCCP

Accepted Manuscript

ROYAL SOCIETY OF CHEMISTRY

www.rsc.org/pccp

Journal Name

ARTICLE

Synthesis and investigation of intra-molecular charge transfer state properties of novel donor-acceptor-donor pyridine derivatives: The effects of temperature and environment upon molecular configurations and the origin of delayed fluorescence

Received 00th January 20xx,
Accepted 00th January 20xx

DOI: 10.1039/x0xx00000x

www.rsc.org/

Murat Aydemir,[a†] Gulcin Haykir,[b] Figen Turksoy,[b] Selcuk Gumus,[c] Fernando B. Dias [a] and Andy P. Monkman [a]

A novel series of donor-acceptor-donor (D-A-D) structured pyridine derivatives were synthesised and detailed photo-physical investigations made using mainly steady-state and time-resolved spectroscopy techniques at varying temperatures. The investigations showed that the molecules have solvent polarity and temperature dependent excited-state configurations, confirmed in two different polarity solvents (295-90 K), i.e. methyl cyclohexane (MCH) and 2-methyltetrahdrofurane (2-MeTHF). In MCH, the investigations revealed dual fluorescence over the temperature range of 295-90K. At 295 K, the ground-state configuration of the molecules have a partially twisted geometry as determined by DFT calculation, yet the emission originates totally from a locally excited (LE) state, however once the temperature is lowered to 90K, the twisted molecular configuration is stabilised, and the emission originates from a fully-relaxed intramolecular charge transfer state (ICT), this is contrary to the systems where structural reorganisation stabilises ICT and this is frozen out at low temperatures. The DFT calculations revealed different ground state molecular configurations due to the presence of the different electron-donating groups, e.g. the molecule including anthracene groups has a near 90^0 twisted geometry whereas the triphenylamine including molecule has a pyramidal geometrical folding, therefore, the decrease in temperature restricts the donor degree of rotational freedom. In 2-MeTHF solution, the fluorescence spectrum of both molecules are always of ICT character, but gradually red-shifts through the fluid to glass transition temperature (~135 K), in this case, the fluorescence occurs after structural and solvent-shell relaxations, however, upon cooling below 135 K, the spectra dramatically shifts back to the blue giving rise to strong emission from an ICT excited-state (but not the LE state) where the molecules have unrelaxed geometries. This significant change in the nature of the emitting species was explained with specific solvent-solute dynamic interactions in the vicinity of the solvation shell and the effect of thermal excitation of molecular vibrational modes of the C-C bond linking donor and acceptor units, Finally, we confirmed that the molecules have ICT ground-state geometry in the solid-state phase (spin-coated films), and the time-resolved decay dynamics were investigated comparing the spin-coated films (at RT and 25 K) and MCH solutions (at 295K and 90 K).

Introduction

Organic light-emitting diodes (OLEDs) have attracted a great deal of interest due to their potential applications in display and illumination technologies.[1–3] Over the past two decades, demanding commercial applications have paved the way for improving the performance of OLEDs. Several approaches have been developed to yield highly efficient devices, either by designing complex OLED structures or synthesising new organic emitters to enhance the brightness and the full-colour emission of OLEDs. [4,5] Donor-acceptor (D-A) type organic molecule architectures are of growing interest for third-generation OLEDs, [6–11] as well as have promising applications in photochemistry [12] and photobiology, [13] due to their unique intramolecular charge transfer properties. Recently, these ICT state properties of molecules have been used as an effective alternative way to achieve high efficiency in OLEDs without using heavy atom containing phosphorescent emitters. [9,14,15] The common potential limitation on the efficiency of the OLEDs are light out-coupling and the intrinsic quantum mechanical spin statistics of charge recombination, which places a limit of 25% singlet exciton production through spin-dependent charge recombination [16,17] which dictates that singlet and triplet excitons are formed in the ratio of 1:3,

[a] Institute of photonic materials, University of Durham, South Road, DH1 5US, UK
[b] TUBITAK Marmara research centre, Chemistry Institute, Gebze, TURKEY
[c] Department of Chemistry, Faculty of Science, Yuzuncu yil University, Van, TURKEY
†Corresponding author, e-mail: murat.aydemir@durham.ac.uk
Electronic Supplementary Information (ESI) available: [details of any supplementary information available should be included here]. See DOI: 10.1039/x0xx00000x

therefore, the maximum internal efficiency of OLED is limited to 25%. [18] Adachi et al.[19] showed how the emissive singlet exciton limitation could be exceeded by means of using phosphorescent heavy metal complexes increasing the emission yield ~100% with harvesting both singlet and triplet excitons. However, these heavy metal containing organo-metallic complexes (generally containing Ir or Pt) are expensive and Ir is the 4th rarest element known, also, this approach is still unconvincing for deep blue emission which also require a high triplet level hosts. To overcome such restrictions, alternative triplet harvesting mechanisms were introduced, e.g. triplet-triplet annihilation (TTA) [20,21] and thermally activated delayed fluorescence (TADF). [7,22] With the TTA mechanism, the maximum achievable singlet yield is 62.5% [20] which still remains an unsatisfactory process for highly efficient OLEDs. However, It is possible to get high efficiency in OLEDs [15,22,23] with materials having a charge transfer excited state that achieve a very small electron exchange energy so that singlet and triplet ICT states become near degenerate so that thermal excitation enables efficient reverse intersystem crossing (rISC) occur to harvest triplet CT states back to emissive singlet CT manifold. This pathway can achieve 100% singlet yield without using phosphorescence materials.[14] This new TADF triplet harvesting mechanism is very promising but as yet our understanding of ICT molecules, especially in the solid state is not very advanced and it is difficult to design ICT emitters that yields 100% efficient OLEDs.

In principle, the donor-acceptor systems containing moieties with different electron donating groups give rise to the molecule with strong charge transfer character. Upon photoexcitation of the donor (D) or acceptor (A) fragment of the molecules, the primary local excited state (LE state) undergoes intramolecular electron transfer from D to A (or vice versa) which is often accompanied by structural relaxations to form a new stabilized dipolar state which is usually called a charge-transfer (CT)/ICT state or exciplex, by means of relative folding of the $D^{\delta+}$ and $A^{\delta-}$ moieties. In principle, oppositely charged radical ions can inherently come close together, termed the *'harpooning effect'* which particularly happens between flexibly bonded donor-acceptor moieties, [24,25] and accompanied by conformational changes to form a dipolar ICT state, as reported previously either in high-polarity solvents and rigid environments.[26, 27] These newly formed ICT states have their own photo-physical properties, and molecular structures as a result of twisting, pyramidisation (wagging), bending or planarization of the excited state geometry. [28] Well-explored example of the intramolecular structural changes accompanying ICT are the formation of twisted charge transfer state (TICT) by means of 90^0 twist of donor groups, [29–32] and formation of a stabilised charge transfer state by a pyramidal distortion (WICT) [33] which have been observed particularly in single bonded D-A type compounds. [30, 34, 35] The primary characteristic of TICT and WICT molecules is that the ICT excited-state can be stabilised over the locally excited-state (LE) by means of twisting/wagging around a single bond which is strongly dependent on solvent temperature and polarity. In principle, once the bridge between the decoupled moieties is only one C-C single bond, the relative conformational folding between $D^{\delta+}$ and $A^{\delta-}$ units is precluded because of the limited degree of vibrational movement in space, which gives rise to a torque and internal rotational relaxations around the central C-C bond and concomitantly the lowest unoccupied molecular orbital (LUMO) is twisted to an angle of 90^0 with respect to the highest occupied molecular orbital (HOMO) stabilising significant amount of D to A charge transfer. [36] One of the remarkable features of TICT/WICT systems is observation of dual fluorescence, mainly originating from both LE and ICT states, but not always the dual emission is observed in TICT states depending on the competition between all the rates involved in different solvents. [37] The emission from the ICT excited-state takes place at lower energy (compared to the LE emission) giving rise to a red-shifted, broadened and unstructured second emission peak along with the LE emission. In such systems, the environmental conditions, e.g. solvent polarity, temperature, viscosity and hydrogen bonding, [28,32,38] play a crucial role on the degree of TICT/WICT excited-state formation. In non-polar solvents, starting geometry of the molecules might be planar depending on the molecules and stays in the ground-state equilibrium conformation; once the environmental factors are changed, particularly temperature, the molecules undergo an intramolecular twisting/wagging conformational reorganisation on excitation resulting in stabilisation of the charge transfer state and concomitant longer-wavelength emission, and the temperature dependent second fluorescence appears. TICT/WICT excited-state formation is strongly favoured in polar solvents, [39] however, the nature of emitting species and their temperature dependencies are more complex in polar solvents. The role of specific solvent-solute interactions play a significant role on the nature of excited-state charge distribution, [40] in particular, the solvent molecules reorient themselves in the vicinity of solute molecules with decreasing temperatures, [41] and excited-state energy is transferred from solute to solvent, so that the fluorescence peak exhibits a thermally-activated and solvent polarity assisted behaviour. [42] However, for potential use in optical devices, ICT emission has to be stabilised in the solid state. Here, there is no solvent to help stabilise the ICT and therefore it is vital to find D-A systems that take up substantially the correct molecular structure in the ground state which stabilises ICT formation upon excitation. Thus, very different behaviour compared to that found in solution is required, and here we explore a family of new materials (all molecular structures are given in Fig. 1, however, according to our photo-physical results, we particularly focused on mainly the most promising molecules, 5a and 5b) that do yield strong ICT emission in solid state and using these new materials we compare solution and solid state behaviour to determine the key molecular geometries and

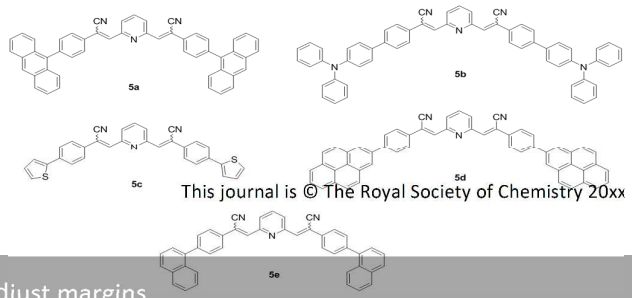

degrees of freedom required to give solid state ICT emission.

Figure 1 Molecular structures of the pyridine emitters

Experimental

Absorption and emission spectra were collected using UV-3600 double beam spectrometer (Shimadzu), and both Fluoromax amd Fluorolog fluorescence spectrometers (Jobin Yvon). All solvatochromic measurements were taken in air saturated solutions using with 1cm depth quartz cuvvettes. In the case of degassing solutions, 3 freezes thaw cycles have been done using a long necked quartz degassing cuvette. The spin-coated films were prepared at 15 mg/ml concentrations and 500 rpm conditions. Time-resolved nanosecond gated luminescence measurements were performed using a high energy pulsed Nd:YAG laser excitation (SL312, EKSPLA) emitting two harmonics at 2.33 eV (532 nm) and 3.49 eV (355 nm) pulse duration is approximately 150 ps, and more details about the nanosecond time-resolved spectroscopy can be found elsewhere. [43] The energy per pulse was chosen around 100 μJ. All drop-casted film measurements were performed under a dynamical vacuum of $<10^{-4}$ Torr using displex helium cryostat.
Picosecond time-resolved fluorescence decays were collected using the time-correlated single photon counting technique (impulse response function, IRF: 26 ps). Vertically polarized picosecond Ti:sapphire laser (Coherent) was used as an excitation source and the excitation wavelength was 402 nm, and the emission was collected using a polarizer at magic angle (54^0), which is crucially important to get rid of polarization effects, and detected by a double monochromator (Acton Research Corporation), and coupled to microchannel plate photomultiplier tube (Hamamatsu R3809U-50).

Results and discussion

Synthesis Section

The synthetic routes for the compounds, **5a-e,** are shown in Scheme 1. The synthesis began with preparing gα,β-diarylacrylonitrile pyridines (**3**) from the Knoevenagel condensation reaction between 2,6-Pyridinedicarboxaldehyde **(1)** and 4-Bromophenylacetonitrile **(2)** with NaOH and absolute EtOH. For introduction of the cyano-group at the vinylic double bond the Knoevenagel condensation is the most common reaction type. [44]
In the second step compound **3** was coupled with various boronic acids to afford a series of α,β-diarylacrylonitrile derivatives containing both anthracene, triphenylamine, thiophene, pyrene and naphthalene unit by the Suzuki cross-coupling reaction. Palladium-catalysed cross coupling reaction is widely used in the construction of aryl C-C bond. Suzuki cross coupling of aryl halides and aryl boronic acids is a powerful method for the synthesis of biaryl compounds. All 5a-e compounds were purified by flash column chromatography with yields ranging from 50 to 77 %. The target molecules 5a-e were characterized by FTIR, NMR (1H-, 13C-) and HRMS (for details see SI). We presume that a compound 5a-e would afford an E,Z isomer mixture such as that observed for nitriles form aromatic aldehyde. [45] The presence of (E,Z)-diarylacrylonitrile in 5a-e were also confirmed by 1H-NMR, in which one singlet for CH=CCN were observed at similar chemical shifts (7.63 and 7.90 ppm), more details can be found in SI.

Scheme 1.

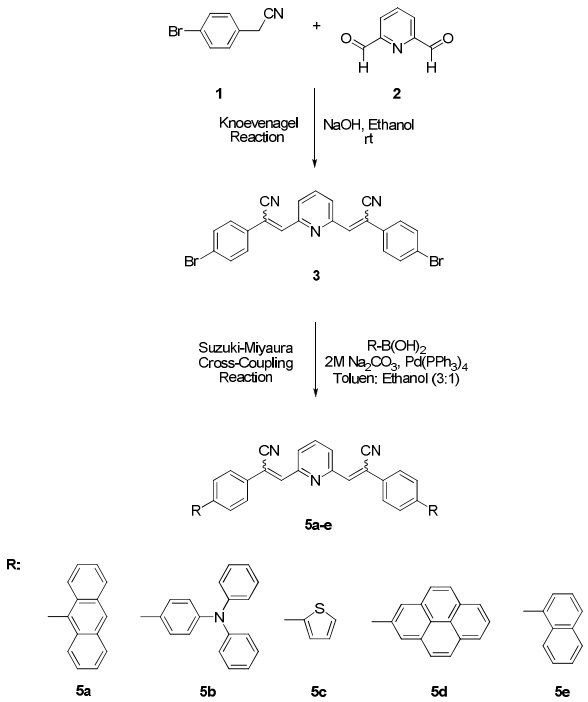

Scheme 1

Electrochemical properties

Electrochemical properties of **5a-e** were investigated by cyclic voltammetry. Cyclic voltammetry was performed in CH_2Cl_2 containing 0.1 M tetrabutylammonium perchlorate at room temperature. **5a, 5c, 5d** and **5e** showed irreversible oxidation processes in the range between 1.05 and 1.55 V, whereas **5d** was reversible (0.83 V) due to the presence of anthracene groups. The HOMO energy levels were calculated from oxidation potential using ferrocene as a standard referenced to the energy level of ferrocene (4.8 eV below the vacuum level) [46] and the LUMO levels were estimated by subtracting the band-gap energy (calculated from the extrapolation of the long wavelength) from the HOMO level. Full details about electrochemical properties of all molecules are given in SI.

The method of DFT calculations and interpretation

The geometry optimizations of all the structures leading to energy minima were achieved by using the density functional theory (DFT) [47,48] at the level of B3LYP/6-31G(d,p) with no

symmetry restrictions. The exchange term of B3LYP consists of hybrid Hartree–Fock and local spin density (LSD) exchange functions with Becke's gradient correlation to LSD exchange. [49] The correlation term of B3LYP consists of the Vosko, Wilk, Nusair (VWN3) local correlation functional [50] and Lee, Yang, Parr (LYP) correlation correction functional. After geometry optimizations, single point calculations at the same level were performed to obtain accurate frontier molecular orbital energy values. All the bond lengths were thoroughly searched in order to find out whether any bond cleavage occurred or not during the geometry optimization process. All these computations were performed by using Gaussian 09 package program. [51]

Frequency analysis for each compound did not yield any imaginary frequencies, indicating that the structure of each molecule corresponds to at least a local minimum on the potential energy surface. The normal mode analysis was performed for 3N-6 vibrational degrees of freedom, N being the number of atoms forming the corresponding molecule.

The time-dependent density functional theory (TD-DFT-B3LYP/6-31G(d,p)) calculation was used to obtain the vertical excitation energies, oscillator strengths (f) and excited state compositions in terms of excitations between the occupied and virtual orbitals for novel compounds. [52, 53] In this study, the TD-DFT method with the same basis set was performed to obtain absorption wavelengths and the oscillation strength (f) within visible to near-UV region.

The conformational analysis through the pyridine and the substituents bond yielded the minimum energy geometry where the cyanine groups are directing opposite sides of the structure. For all systems, the head part (pyridine-double bond) are found to be planar, whereas the tail (aromatic substituents) parts are tilted towards the main plane due to geometrical reasons resulting an interruption of π-conjugation within the molecule. However, the planarity throughout the molecule is not distorted that much for thiophene susbstituent (**5c**).

The most important design consideration of ICT molecules showing TADF is to obtain a small energy gap between the S_1 and T_1 states (ΔE_{ST}). A molecule meets this requirement only when its lowest-energy transition has a small singlet–triplet exchange energy. Current trends in research of novel ICT systems are mainly focusing on intramolecular donor-acceptor (D-A)-type molecules. Therefore, appropriate donor-acceptor units have to be selected carefully to obtain full-color ICT molecules, with their HOMO and LUMO being localized on different constituents of the structure. To obtain details about the geometric and electronic structures of **5a–5e**, time-dependent density functional theory (TD-DFT) calculations were performed at the B3LYP/6-31G(d,p) level. The HOMO, LUMO energies and the energy gap between singlet and triplet excited states for compounds **5a–5e** are given in Table 1, and the 3D frontier molecular orbital schemes can be seen in Fig. 2. All molecules except for **5c** exhibit clear separation of the HOMO and LUMO distributions. As shown in Fig. 2, for compounds 5a–5e, the LUMO is mainly located on the head part (electron-accepting pyridine core), whereas the HOMO is predominantly localized on the electron-donating anthracene, triphenylamine, naphthalene and pyrene substituents, because of the highly twisted geometry between the donor and acceptor constituents. The thiophene substituent is an exception, in which both HOMO and LUMO located throughout the molecule since the conjugation is not disturbed due to loss of planarity.

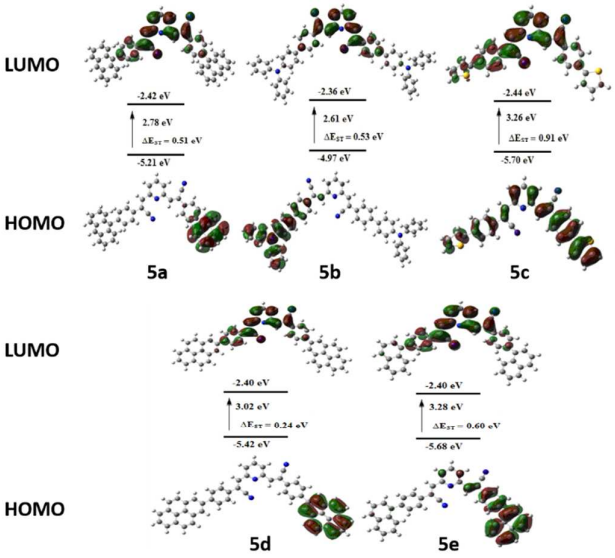

Figure 2 Frontier-molecular-orbital distributions, energy levels and energy gaps (ΔE_{ST}) between S1 and T1 for compounds 5a–5e, characterized by TD-DFT calculations

	HOMO	LUMO	ΔE	ΔE_{ST}
5a	-5.21	-2.42	2.79	0.51
5b	-4.97	-2.36	2.61	0.53
5c	-5.70	-2.44	3.26	0.91
5d	-5.42	-2.40	3.02	0.24
5e	-5.68	-2.40	3.28	0.60

Table 1: Frontier molecular orbital energies (B3LYP/6-31G(d,p)). All energies are in eV.

Steady-state measurements

Fig. 3 shows the normalized absorption and fluorescence spectra of molecules (5a and 5b) at RT, the concentrations

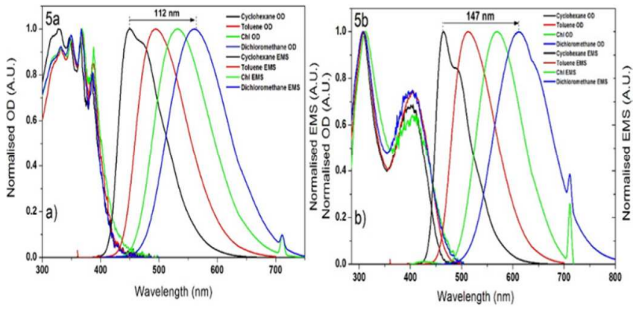

were chosen close to each other, 7.2 x10^{-6} M for 5a and 6.1 x10^{-6}M for 5b. The broad range solubility of these materials offers us a chance to study the optical properties in variety of solvents (from non-polar to polar range), e.g. cyclohexane, toluene, chlorobenzene and dichloromethane

Figure 3 Normalised absorption and photoluminescence spectra in different polarity solvents at RT **a)** 5a **b)** 5b. All steady-state measurements were taken using 355nm excitation wavelength, the concentrations were 7.2 E-6 M , 6.1 E-6 M for 5a and 5b, respectively.

In molecules, n-π^* and π-π^* transitions can be distinguished by the effect of solvent polarity on the energy of the excited and ground states. Increasing solvent polarity shifts the emission spectra to the blue in the case of n-π^* transitions, whereas the spectra shifts to red when the transition is π-π^* character. Here, the structure of the emitters consists of similar electron acceptor units at the central position (aromatic pyridine cyano group) that contains robust C-N bonds serving as electron-withdrawing units, whereas both side arms contain different electron-donating groups (anthracene and triphenylamine). As seen in Fig.3, the substitution of triphenylamine group by anthracene group further red-shifts the emission spectra, however, in absorption spectra, the π-π^* transition peaks (ca. 367 nm for 5a and ca. 401 nm for 5b) do not deviate with increasing polarities. The negligible bathochromic shift in absorption spectra with increasing solvent polarities (non-polar cyclohexane to polar dichloromethane) is consistent with a small difference between the dipole moments of Franck-Condon excited and ground states. Therefore we surmise that the absorption spectra of each molecules arises totally within the diarylacrylonitrile pyridine unit (A), whereas the fluorescence spectra which show solvent polarity dependent behaviour (loss of structure and strongly red-shifted as increasing solvent polarities) clearly indicate that solvent-solute interactions stabilise the intramolecular charge transfer (ICT) excited-state, yielding a dipole moment, in the ICT excited-state, that is larger than that in the ground state.

In principle, upon excitation, the various combinations of donor groups result in different electron density distribution towards the acceptor unit as a result of environment dependent effects (e.g. solvent polarity and temperature), mutual conformations of $D^{\delta+}$ and $A^{\delta-}$ species, leading to the formation of ICT excited-states with various charge transfer character strengths. In general, the photo-physical properties of molecular systems with an ICT excited-state show a large red-shifted emission as the polarity of the solvent increases.[54] The strength of an ICT excited-state is associated with solvatochromic shifts, the largest positive solvatochromic shift is typically associated with the material that has the strongest ICT character. From this point of view, the strongest electron density accumulation on the A^- moiety (diarylacrylonitrile pyridine) was observed among 5a and 5b molecules by substituting the D^+ units with anthracene and triphenylamine groups resulting in substantial charge redistribution which accompanied by the largest solvatochromic shifts, 112 nm for 5a and 147 nm for 5b (see SI of solvatochromic shifts of other donor groups) and the ca. 35 nm more positive red-shift can be interpreted in terms of better electron-donating ability of triphenylamine groups.

The steady-state fluorescence spectra of 5a and 5b were collected as a function of temperature (see in Fig 4.) in non-polar (MCH) solvent in the range from 295- 90 K. In MCH, at RT, we observe clear well-structured emission characteristic of an excitonic LE state emission; as the temperature is lowered from 295 K to 90 K, we observed gradually loss of the resolved fluorescence band, at the same time the appearance of an unstructured and red-shifted emission (see Fig. 4 a. b.) originating from a newly formed state (not originating from possible aggregations, see concentration dependent spectra in SI) indicative of '*charge transfer*' characteristics. With the appearance of dual fluorescence at lower temperatures, we ascribed this effect to be caused primarily by decreasing vibrational excitation of the molecules which otherwise destabilises the twisted geometry between donor and acceptor units.

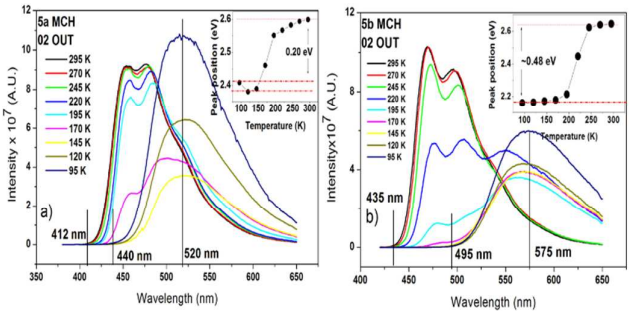

Figure 4 a) Temperature dependence of steady-state corrected phototoluminescence spectra in MCH **a)** 5a **b)** 5b

In MCH, the ground state conformation of the molecules is 'twisted', i.e. twisted molecular configuration of the anthracene moiety (5a) and pyramidal distortion ('*wagged*') molecular configuration of triphenyamine moiety (5b) with respect to the neighbouring phenyl ring. At 295 K, the solvent viscosity and polarity are not sufficient to stabilise this twisted configuration over thermal fluctuations (rotations about the

centre of C-C single-bond) which help to drive the molecule planar and conjugated in the excited state causing the fluorescence to be emitted only from the (planar) locally excited state (LE). However, as the temperature of the solvent decreases, the ground state molecular structural is stabilised by increased solvent viscosity and decreasing temperature, i.e. the conformation is stabilised due to the stiffening of the active intramolecular rotations and vibrations around the centre of C-C single-bond of the D^+ groups (anthracene and triphenylamine) to retain the twisted/wagged geometry, (see charge distribution graph in Fig.5). It can be seen in the emission spectra, Fig 4, that the ICT band does not further relax (to lower energy) with decreasing temperature, this very important observation we ascribe to the fact that the solvent is non polar such that even as the temperature is decreased no

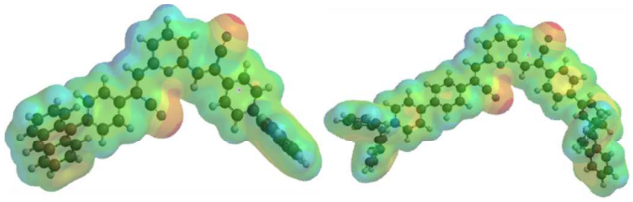

5a **5b**

significant increase in polarity is achieved, and so, no solvent induced relaxation of the ICT state occurs, thus we only observe the ICT in the initial ground state geometry of the molecules. This reveals the subtle control played by the solvent environment on conjugation versus a twisted broken conjugation geometry.

Figure 5 Charge distribution graphs for 5a and 5b showing perpendicularly positioned anthracene unit (5a) and and pyramidal distortion (wagged) conformation of triphenylamine unit (5b) with respect to the phenyl ring referring to possible orientations of molecules in their ground states.

Theoretically, if the linkage between the decoupled moieties is only one single bond, the relative conformational folding between $D^{\delta+}$ and $A^{\delta-}$ units are precluded because of limited degree of freedom in space, therefore, the internal rotational relaxations around the central bond are favored and concomitantly the $D^{\delta+}$ moiety takes an out of plane position with respect to the $A^{\delta-}$ moiety which results in a change in the electronic distribution by means of forming relaxed excited stated. [28] However, once the temperature drops below the fluid to glass transition of MCH (<135 K), the rigid nature of matrix prevents any donor rotations around the single bond of phenyl ring which gives rise to complete disappearance of LE fluorescence band (collapse of the LE band as a function of temperature), thus, the fluorescence only originates from TICT excited-state for 5a and from WICT excited state for 5b which can be considered as a final retention of twisted/wagged ground state conformation of molecules. [55]

In addition, the photo-physical investigations were also made in a rigid host matrix to understand the ground-state conformations of the molecules in the solid-state phase. Steady-state measurements were taken at RT using drop-casted films (including 10 % CBP host material. see Fig.6 a. b.). In such rigid matrix, the molecules do not have rotational degrees of freedom, therefore, possible corresponding rotations about the C-C bond will be prevented, and the emission spectrum should not exhibit the effect of significant structural reorganisation. Spectra confirm that the ground-state conformations of the solid-state phases have twisted/wagged geometry as the emission peak positions (ca. 524 nm for 5a and ca. 580 nm for 5b) are in very good agreement with the emission positions of the ICT excited-state observed in the rigid MCH matrix (ca. 520 nm for 5a and ca.575 nm for 5b) at 90 K. The solid-state spectra also only showed slight temperature dependent behaviour (slightly red-shifted) comparing at RT and 25 K again confirming no increased structural relaxation as a function of decreasing temperature, as will be represented in time-resolved spectroscopy measurements section below.

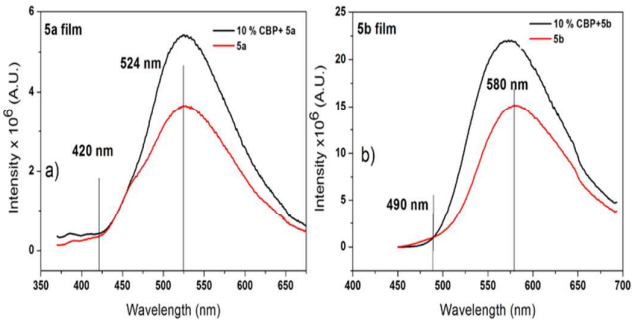

Figure 6 The steady state spectra of dropcasted film including 10 % CBP host material a)**5a** b) **5b**

We carried out analogous studies of these molecules in polar 2-MeTHF solution in the temperature range from 295 K to 90 K. [41] From our steady-state measurements in 2-MeTHF solution it is clear that the thermochromic red shift and associated decreasing quantum yield (also there is not significant triplet contribution on ICT state, see Table 2) occurs with decreasing temperature, indicative of further relaxation of the excited-state geometric distortion and increased charge transfer strength as the temperatured decreases. The fluorescence spectrum red-shifts through the fluid to glass transition temperature (~135 K), in this case the fluorescence has taken place after full solvent-relaxation, but then, upon cooling the temperature further (<135 K) the spectra start shifting to the blue again (see in Fig. 7)

Below 135 K, intramolecular rotations about the single C-C bond are inhibited because of the increasing rigidity of the 2-MeTHF matrix environment. At low temperatures the solvent shows high viscosity and there is less thermal activation of molecular vibrations which plays a significant role on solvation

dynamics. Once the solvent freezes (e.g. at 90 K), a very large blue-shifted fluorescence peak is observed (ca. 478 nm for 5a

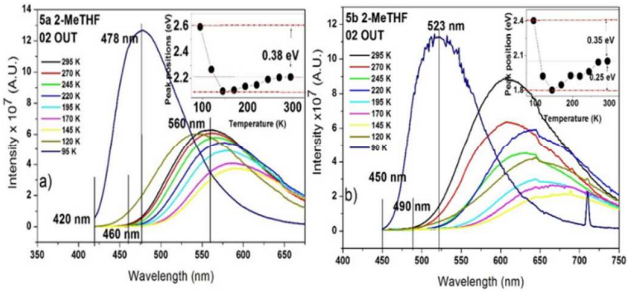

and ca. 520 nm for 5b) however, the band is still a structureless gaussian shape (to the red of the LE band seen in MCH) and so we ascribe this 'blue band' to the non-relaxed ICT state, in a rigid polar environment, corresponding to that seen in MCH at low temperature. Our findings are in agreement with previous reports of 2-MeTHF solvent relaxation dynamics,[41,56,57] where similar fluorescence behaviour trend upon decreasing temperatures were reported.

Figure 7 a) Temperature dependence of steady-state corrected phototoluminescence spectra in 2-MeTHF **a)** 5a **b)** 5b

The general conclusion from all this work is that the temperature has significant effect on the '*polarity and polarizability*' of 2-MeTHF solvent in the vicinity of solute, which results in decreasing '*permittivity*' of solvent as reported by Kawski et al. [58] In principle, the existence of dipoles in solute give rise to charge orientations of solvent molecules in the vicinity of solute which appears as the ICT excited-state dipole moment reorientation (generally rotational relaxations) of the solvent dipoles giving rise to increase in effective solvent polarity and greater degree of charge stabilisation in the solute molecule, and this effect will be more enhanced as the temperature decreases. [41] According to the Gorlach *et al*. [56] if the solvent reorientation occurs on a time scale which is comparatively as fast as the fluorescence lifetime of solute, then it is possible to observe gradually red-shifted fluorescence maxima (thermochromic shift) upon decreasing temperatures, therefore, between fluid to glass temperature regime the spectra of our molecules show gradual thermochromic shift. However, once the temperature is lowered below 135 K, the thermochromic shift decreases due to the slowing of the re-orientation of the solvent molecules in the vicinity of the ICT excited-state dipole as the motion of the solvent molecules is slowed in the rapidly increasing viscous solvent shell. Below the freezing point, the solvent molecules can no longer reorient and the fluorescence 'dramatically' blue-shifts to the energy of the non-relaxed ICT state. The effect should also been observed by time dependent stokes shift as measuring an increase in solvent (2-MeTHF) relaxation time from nanosecond range (>135 K) to seconds (<135 K, e.g. 90 K). [56]

2.5 Time-resolved measurements

In 2-MeTHF, the twisted excited state can be stabilized with respect to a planar local excited state, hence, the emission spectrum show strongly red-shifted and broadened fluorescence which arise from excited-states of the molecules having strong charge transfer character. The fluorescence lifetimes were measured (see Fig. 8) by time correlated single photon counting (TCSPC) method for 5a and 5b under varying conditions (in MCH and 2-MeTHF) to assess the relative importance of solvent polarity on the fluorescence decays. The molecules in MCH solution were excited at 368 nm and the emission from LE state was collected at 450 nm and 475 nm for 5a molecule and at 470 nm and 500 nm for 5b molecule. The LE emission of molecules shows biexponetial decay components, one long lasting and one fast decay (see SI for details). The large lifetime differences between the two components indicate that they are of different origin. The long lasting component correspond to the LE emission and the fast component may result from partially twisted geometry of the molecues giving rise to a fast non-radiative decay channel. For all analysis, we have used global analyzes programme to calculate the fluorescence lifetimes of molecules using deconvolution of the apparatus response function.

The molecules in 2-MeTHF solution were excited at 402 nm and the emission was collected at 500 to 650 nm for both molecules and the data are presented in Table 2. Obviously the fluorescence decay of molecules in a polar environment have a different nature due to the difference in arrangement of molecular geometries. The measurements clearly indicate that the lifetimes of ICT excited state have reduced significantly comparing the lifetime decays in MCH which is expected behaviour from ICT excited state decaying faster than the LE state. [59] The ICT fluorescence shows triexponetial decay components (at 500 and 550 nm) for 5a molecules, then turns into biexponential at 600 and 650 nm. The slow component can be associated with the TICT state and the rest fo the fast components are of diffent origins. And similar behaviour was observed with 5b molecule, triexponential decay components turn into biexponential at 650 nm. In our understanding, the fast component at shorter wavelengths may be associated with rapid quenching channels of the molecules that do not reach the stabilised CT geometry.

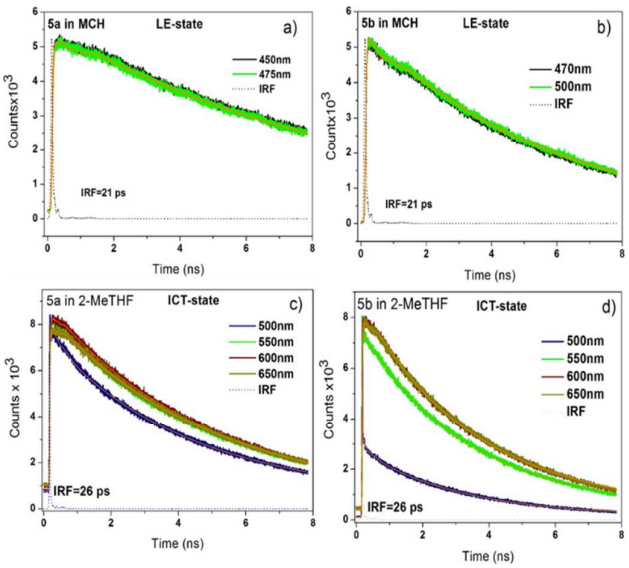

Figure 8 The fluorescence lifetime decays were collected by using single photon counting technique at different wavelength positions in degassed MCH (**a** and **c**) and 2-MeTHF solutions (**c** and **d**) at RT. The Orange segmented lines are exponential fits

Materials	Quantum Yields (Φ_{ICT}) In 2-MeTHF Air saturated/ Degassed (%)	λ_x= 402 nm In air-saturated 2-MeTHF			
		500 nm	550 nm	600 nm	650 nm
5a	27.5 ± 3 /35.6 ± 4	τ_1= 3.76 ns A1=0.25 τ_2= 0.25 ns A2=0.05 τ_3= 6.4 ps A3=0.43 χ^2= 1.12	τ_1= 3.92 ns A1=0.23 τ_2= 0.1 ns A2=0.03 τ_3= 8.8 ps A3=0.02 χ^2= 1.17	τ_1= 4 ns A1= 0.24 τ_2= 0.06 ns A2=0.02 χ^2= 1.2	τ_1= 4.04 ns A1=0.23 τ_2= 0.04 ns A2=0.014 χ^2= 1.22
5b	20.7 ± 2 /26.2 ± 4	τ_1= 3.04 ns A1=0.30 τ_2= 0.22 ns A2=0.08 τ_3= 3 ps A3=5.85 χ^2= 1.08	τ_1= 3.18 ns A1=0.30 τ_2= 0.15 ns A2=0.05 τ_3= 6.3 ps A3=0.44 χ^2= 1.1	τ_1= 3.28 ns A1=0.30 τ_2= 0.08 ns A2=0.04 τ_3= 4.5 ps A3=0.01 χ^2= 1.15	τ_1= 3.32 ns A1=0.30 τ_2= 0.08 ns A2=0.03 χ^2= 1.2

Table 2 The quantum yields and fluorescence lifetime decays of ICT excited-state were measured for 5a and 5b in 2-MeTHF solution, and triplet state contribution on total fluorescence was elucidated by degassing the solution.

In order to support our measurements above, we have additionally used nanosecond gated time resolved spectroscopy technique to measure the decay dynamics in MCH solution and the results compared with the spin-coated films. By way of this technique we are able to record more than 12 orders of magnitude in intensity and more than 10 decades of time in one single experiment, [43] therefore, it is possible to measure lifetime decays with totally covering both prompt (PF) and delayed fluorescence (DF) regimes simultaneously (in one curve) as shown in double logarithmic scales in Fig . 9.

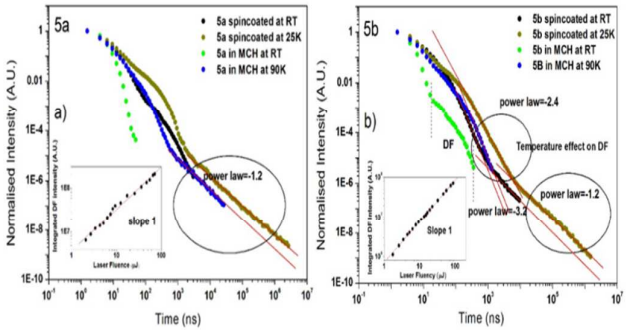

Figure 9 Log-log scale the lifetime decays **a)** 5a in MCH solution (both at RT and 90 K) and spincoated film (both at RT and 25 K) **b)** 5b in MCH solution (both at RT and 90 K) and spincoated film (both at RT and 25 K)**,** the laser fluence dependence of DF were inserted into the graphs

In general, the initial fast part of the decay is assigned to PF, and the long slower decay component is assigned to DF, in particular, Fig. 9 a and b. include the lifetime decay of 5a and 5b either in degassed MCH solution (at RT and 90K) and spin-coated thin film (at RT and 25 K). In MCH, at RT, the lifetimes of PF were measured as 4.1±0.07 ns for 5a and as 3.5±1 ns for 5b which were emitting from the LE state as identified from the spectrum of the emission during this time (Fig. 10 a and b), note that at RT, the DF was only measured for 5b material as 49.85 ±0.8 ns, but not for the 5a material. At 90 K, as seen in the steady state spectra, the molecules have a stabilised twisted/wagged geometry which can be confirmed with the time resolved spectra showing an unstructured, red-shifted and much broadened CT type emission comparing with the structured spectra at RT, clearly emission emanating from the TICT/WICT excited-states at all decay times. However, at 90 K, the measured lifetime decays represented the dynamics of the ICT states, resulting in biexponential PF decay dynamics; $\tau_{1=}$ 7.8± 0.5 ns, τ_2=53.46±1.8 ns for 5a and $\tau_{1=}$ 4.39± 0.28 ns, $\tau_{1=}$ 30.47± 1.9 ns for 5b. Then the decays transform into a power law (decay) regime ($I_{DF} \sim t^{-m}$) at longer times with an exponent of -1.2 for 5a and -3.2 for 5b. No phosphorescence emission could be observed for both of the materials at 90 K.

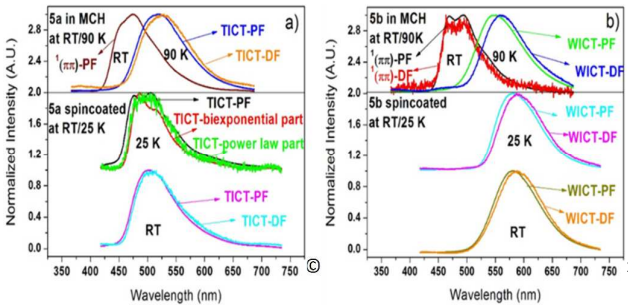

Figure 10 Time-resolved spectra of materials in MCH (at RT and 90 K) and spincoated film (at RT and 25 K) **a)** 5a **b)** 5b

Fig. 9 a. b. are also given the spectra at different decay times of spin-coated thin films for 5a and 5b at RT and 25 K. The lifetimes of PF were measured as $\tau_{1=}$ 4.88 ±0.28, $\tau_{2=}$ 15.17± 0.93 ns for 5a and $\tau_{1=}$ 6.76± 0.49 ns, $\tau_{2=}$ 31.82± 1.27 ns for 5b at RT. The DF follows a biexponential lifetime decay for 5a at RT with $\tau_{1=}$ 111.2 ±3.9 ns and τ_2 = 430.74 ± 11.7 ns decays (which is distinctive, because no DF was observed for 5a in MCH solution at RT), whereas the DF from 5b follows two power law regimes with the exponent of -3.2 then turns to -1.2 at later times at RT. Once the temperature was lowered to 25 K, the PF lifetimes increased showing biexponential dymanics τ_1=11.55 ±0.73 ns, τ_2=165.54 ±3.97 ns for 5a and τ_1=5.81±0.34 ns, τ_2=62.8±2.86 ns for 5b. The DF of 5a decays following the transition from biexponential to power law regime ($I_{DF} \sim t^{-m}$) with an exponent of -1.2 (which is intriguing point to note as it is so similar power law behaviour compared with the frozen solution at 90 K). The DF decay of 5b again follows two power law regimes; the DF decays with the exponent of -2.4 at early times of the regime and then turns into -1.2 at later time ranges. Once again no phosphorescence emission could be observed with spin-coated films at 25 K.

In Fig. 10 a and b, we give the spectra observed at different decay times. At room temperature both 5a and 5b PF and DF are nearly identical, clearly ICT in nature. The DF spectra show a hint of a red shoulder that shifts the peak of emission to the red. We have no clear spectral separation of this feature so it is difficult to ascribe it to a phosphorescence component for example, it may be emission from a slightly different geometric ICT state. At 25 K, 5b yields the same behaviour as at room temperature, whereas 5a gives more complex structured PF and DF emission which appears to be some combination of species but well red shifted from LE emission, this tends to shift more to fully ICT emission at longer times. In principle, the appearance of long-lived DF emission (power law regime) at low temperatures could be attributed to enhanced triplet state contribution upon total ICT emission [60] giving rise to DF via two possible mechanisms: triplet-triplet annihilation (TTA) or geminate-pair recombination (GPR).[61–64] In practice, the best ways to distinguish these phenomena is either comparing the decay pattern of phosphorescence and the delayed fluorescence, or measuring the DF intensity dependence upon the laser excitation intensity. If the (delayed) singlet excitons originate from the TTA then the DF decays either exponentially at half the PH lifetime or it shows t^{-2} power law decay dynamics as a result of the dominant bimolecular annihilation process, in addition, singlet generation via TTA mechanism, the DF emission should follow a quadratic (excitation) intensity dependence, at low intensities ($I_{exc} \leq 10\ \mu J$) and then turn over into a linear law at high intensities($I_{exc} \geq 10\ \mu J$). [62] In our case we cannot measure the PH lifetime, therefore, only the DF intensity dependence on laser fluence could be recorded, covering the DF power law regime for spin-coated films at 25 K (2 µs- 70 µs for 5a, 10 µs- 80 µs for 5b) and frozen MCH solutions (1 µs- 10 µs for 5a, 0.1 µs- 1 µs for 5b). In all cases we find a linear (slope 1) dependence upon laser fluency (See Fig. 9 as inserted graph integrated DF intensity as a function of laser fluence) concomitant with a monomolecular decay process, not bimolecular processes as triplet-triplet annihilation.

Alternatively, monomolecular DF can arise from the decay of geminately bound electron-hole pairs. According to Monte Carlo simulations upon geminate pair recombination phenomena [65,66] the electron-hole pairs show dispersive characteristics within their mutual coulombic potential and result in time dependent power law decay $I \sim t^{-m}$ with the value of m=1..1.3 for the delayed fluorescence which is in good agreement with the measured time dependence of 5a and 5b spin-coated film featuring a power law with the exponent of -1.2 at 25 K. In addition, if the geminate pair is generated as a result of bimolecular process, e.g. triplet-triplet annihilation, the DF intensity dependence should follow quadratic to linear intensity dependencies (which is not the case here). The electron-hole pairs here are generated as a result of a monomolecular process, i.e. dissociation of an excited state, with intensity dependence of the DF linear on excitation intensity (from low to high I_{exc} conditions). This behaviour was observed in spin-coated thin films at 25 K as well as in dilute frozen solutions with the same linear power-law dependency of the DF predominantly observed at low temperatures. To confirm the origin of the DF, we measured the laser fluence dependence of DF for 5b material in dilute MCH solution at RT, again it showed the same linear dependency upon I_{exc}. Thus, the major primary dissociation mechanism of excited states into geminate electron-hole pairs in these ICT states is an intramolecular process as reported by Vissenberg *et al.* [67] This also can explain why the quantum yield of emission reduces as the ICT state relaxes (to lower energy). With increased excess energy (the difference between the initial photocreated state and the final ICT state), it will be easier for the delocalised electron hole pair to escape their mutual coulomb attraction and dissociate,[64] if the geminate (and possible non-geminate) recombination process has a poor radiative efficiency then with increasing relaxation the total emissive yield will decrease as the rate of dissociation increases.

4. Conclusion

In conclusion, we have investigated the excited-state photophysical properties of novel family of donor-acceptoras molecules with anthracene and triphenylamine donor units that in the ground state have a large degree of rotation about around the phenyl C-C bond in the ground state. Significant differences in emission spectra properties were observed as a function of temperature (from 295 K to 90 K) in non polar MCH and polar 2-MeTHF solutions. In particular, in MCH, as the temperature is lowered the dual fluorescence appeared and, at RT, the emission only arose predominantly from locally excited state where the ground-state geometry of the molecules have partially twisted or pyramid-shaped of D-A

orientations. In our understanding, although D-A character is significant for TICT/WICT deactivation and also the degree of twist is more important parameter. However, the observation of a resolved emission in MCH at RT showing a planarization in the excited state geometry, therefore, no CT-type emission is observed. However, once the solvent is frozen, and the geometry cannot relax anymore resulting in observation of a broad, CT-type emission confirming that perpendicular arrangement of ground-state D-A is stabilised in the excited state.

By contrast, in 2-MeTHF the fluorescence is always that of the ICT state and the spectrum gradually red-shifts through the fluid to glass transition temperature (~135 K), but then, upon cooling the temperature (<135 K) the spectra significantly shifted to the blue resulting in ICT emission from an unrelaxed molecular geometry, but not the LE state. Thus, only at high temperature and in non polar solvent we do not observe ICT emission, a result also confirmed from solid state measurements where again only ICT emission is observed. This highlights the key role of specific solvent-solute interactions in the vicinity of solvation dynamics where vibrational excitation of the molecule at high temperature coupled with the lack of solvent polarity destabilises the twisted molecular structure to allow planarisation and conjugation to over come ICT formation. In addition, the investigations revealed that the twisted ground-state molecular conformations are retained in spin-coated thin films ensuring ICT stabilisation and emission as required for dominant ICT emission in a device setting. Delayed fluorescence predominantly originated from monomolecular recombination of the geminately bound electron-hole pairs and we believe that this can be a major loss mechanism of quantum yield in ICT systems and particularly as the ICT state moves to lower energy the competition with dissociation becomes acute. It is clear that to achieve ICT excited states in the solid state, the active emitter molecule must have a ground state configuration that stabilises the charge transfer state and this must be 'locked-in' in the solid state.

Acknowledgement

We are thankful to the Ministry of Education of Turkey for supplying PhD scholarship.

Notes and references

1 J.H. Burroughes, *et al.*, *Nature*, 1990, **347,** 539–541.
2 C.Tang, S. Vanslyke, *Appl. Phys. Lett*. **51,** 913–915 (1987)
3 J.Liang, L. Li, X. Niu, Z. Yu, Q. Pei, *Nat. Photonics,* 2013, **7,** 817–824.
4 R. Meerheim, K. Walzer, M. Pfeiffer, K. Leo, *Appl. Phys. Lett.*, 2006, **89,** 061111.
5 L. S. Liao, K.P. Klubek, C. W. Tang, *Appl. Phys. Lett.*, 2004, **84,** 167–169.
6 L. Duan, J. Qiao, Y. Sun, Y. Qiu, *Adv. Mater.,* 2011, **23,** 1137–1144.
7 S.Y. Lee, T. Yasuda, H. Nomura, C. Adachi, *Appl. Phys. Lett.,* 2012, **101,** 093306.
8 S.A. Jenekhe, L.D. Lu, M.M. Alam, *Macromolecules*, 2001, **34,** 7315–7324.
9 V. Jankus, C.-J. Chiang, F. Dias, A.P. Monkman, *Adv. Mater.,* 2013, **25,** 1455–1459.
10 H. Tanaka, K. Shizu, H. Nakanotani, C. Adachi, *Chem. Mater.,* 2013, **25,** 3766–3771.
11 Q. Zhang, *et al.*, *J. Am. Chem. Soc.*, 2014, **136,** 18070–18081.
12 F. Qian, *et al., J. Am. Chem. Soc.*, 2009, **131,** 1460–1468.
13 Y. Suzuki, K. Yokoyama, *J. Am. Chem. Soc.*, 2005, **127,** 17799–17802.
14 F.B. Dias, *et al.*, *Adv. Mater.*, 2013, **25,** 3707–3714.
15 V. Jankus, *et al.*, *Adv. Funct. Mater.*,2014, **24,** 6178–6186.
16 P.W. Atkins, *Molecular quantum mechanics*, 1983, Oxford University Press.
17 Z.H. Kafafi, Z. H., *Organic electroluminescence*, 2005, CRC Press.
18 M.A. Baldo, *et al.*, *Nature,* 1998, **395,** 151–154.
19 C. Adachi, M.A. Baldo, M.E. Thompson, S.R. Forrest, *J. Appl. Phys.*, 2001, **90,** 5048–5051.
20 D.Y. Kondakov, *et al*., *J. Appl. Phys.,* 2009, **106,** 124510.
21 S.M. King, *et al.*, *J. Appl. Phys.*, 2011, **109,** 074502.
22 K. Goushi, K. Yoshida, K. Sato, C. Adachi, *Nat. Photonics,* 2012, **6,** 253–258.
23 Q. Zhang, *et al.*, *J. Am. Chem. Soc.*, 2012, **134,** 14706–14709.
24 E.A. Chandross, H.T. Thomas, *Chem. Phys. Lett.,* 1971, **9,** 393–396.
25 P.R. Brooks, *Mol. Phys.,* 2012, **110,** 1729–1738.
26 M.J. Shephard, M.N. Paddon-Row, *J. Phys. Chem. A,* 2000, **104,** 11628–11635.
27 M. Goes, *et al.*, *J. Phys. Chem. A,* 2002, **106,** 2129–2134.
28 Z.R. Grabowski, K. Rotkiewicz, W. Rettig, *Chem. Rev.,* 2003 **103,** 3899–4031.
29 K. Rotkiewicz, K.H. Grellman, Z. Grabowski, *Chem. Phys. Lett.*, 1973, **19,** 315–318.
30 Z. Grabowski, K. Rotkiewicz, A. Siemiarczuk, D. Cowley, W. Baumann, *Nouv. J. Chim.-New J. Chem.,* 1979, **3,** 443–454.
31 Z. Grabowski, K. Rotkiewicz, A. Siemiarczuk, *J. Lumin.*, 1979, **18-9,** 420–424.
32 W. Rettig, *Angew. Chem.-Int. Ed. Engl.*, 1986, **25,** 971–988.
33 S. Ghosh, K.V.S. Girish, S. Ghosh, *J. Chem. Sci.,* 2013, **125,** 933–938.
34 W. Rettig, R. Gleiter, *J. Phys. Chem.*, 1985, **89,** 4676–4680.
35 W. Rettig, G. Wermuth, *J. Photochem.* **28,** 351–366.
36 W. Li, *et al., Adv. Funct. Mater.,* 2012, **22,** 2797–2803.
37 P.R. Bangal, S. Panja, S. Chakravorti, *J. Photochem. Photobiol. Chem.*, 2001, **139,** 5–16.
38 F.A.S. Chipem, A.Mishra, G. Krishnamoorthy, *Phys. Chem. Chem. Phys.*, 2012, **14,** 8775–8790.
39 J. Lipinski, H. Chojnacki, Z. Grabowski, K. Rotkiewicz, *Chem. Phys. Lett.*, 1980, **70,** 449–453.
40 B. Ladanyi, A. Foriero, *Can. Geotech. J.,* 1998, **35,** 541–559.
41 N.H. Damrauer, J.K. McCusker, *Inorg. Chem.*, 1999, **38,** 4268–4277.
42 M.A. Haidekker, T.P. Brady, D. Lichlyter, E.A. Theodorakis, *Bioorganic Chem.*, 2005, **33,** 415–425.
43 C. Rothe, A.P. Monkman, *Phys. Rev. B*, 2003, **68,** 075208.

44 M. Hanack, B. Behnisch, H. Hackl, R. Martinez-Ruiz, K.H. Schweikart, *Thin Solid Films,* **417,** 2002, 26–31.
45 S. Dibiase, B. Lipisko, A. Haag, R. Wolak, G. Gokel, *J. Org. Chem.*, 1979, **44,** 4640–4649.
46 M. Al-Ibrahim, H.K. Roth, U. Zhokhavets, G. Gobsch, S. Sensfuss, *Sol. Energy Mater. Sol. Cells,* 2005*,* **85,** 13–20.
47 W. Kohn, L. J. Sham, *Phys. Rev.,* 1965*,* **140,** 1133–&.
48 A.H. Larsen, U. De Giovannini, D.L. Whitenack, A. Wasserman, A. Rubio, *J. Phys. Chem. Lett.,* 2013*,* **4,** 2734–2738.
49 A. Becke, *Phys. Rev. A,* 1988*,* **38,** 3098–3100.
50 S. Vosko, L.Wilk, M. Nusair, M., *Can. J. Phys.,* 1980, **58,** 1200–1211.
51 H. Frisch, Y. Nie, S. Raunser, P. Besenius, *Chem. Weinh. Bergstr. Ger.*, 2015, **21,** 3304–9.
52 M.E. Casida, K.C. Casida, D.R. Salahub, *Int. J. Quantum Chem.,* 1998*,* **70,** 933–941.
53 M.E. Casida,C. Jamorski, K.C. Casida, D.R. Salahub, *J. Chem. Phys.,* 1998, **108,** 4439–4449.
54 C. Reichardt, *Chem. Rev.,* 1994, **94,** 2319–2358.
55 C. Dubroca, *Chem. Phys. Lett.* , 1972, **15,** 207–&.
56 E. Gorlach, H. Gygax, P. Lubini, U. Wild, *Chem. Phys.,*1995, **194,** 185–193.
57 G.U. Bublitz, S.G. Boxer, *J. Am. Chem. Soc.,* 1998, **120,** 3988–3992.
58 A. Kawski, B. Kuklinski, P. Bojarski, *Chem. Phys. Lett.*, 2008, **455,** 52–54.
59 R.V. Pereira, A.P.G. Ferreira, M.H. Gehlen, M. H, *J. Phys. Chem. A,* 2005*,* **109,** 5978–5983.
60 S.M. King, R. Matheson, F.B. Dias, A.P. Monkman, *J. Phys. Chem. B,* 2008, **112,** 8010–8016.
61 C. Rothe, S.I. Hintschich, A.P. Monkman, *Phys. Rev. Lett.*, 2006, **96,** 163601.
62 A. Hayer, H. Bassler, B. Falk, S. Schrader, *J. Phys. Chem. A,* 2002, **106,** 11045–11053.
63 A. Koehler, H. Bassler, *Mater. Sci. Eng. R-Rep.,* 2009, **66,** 71–109.
64 M. Aydemir, V. Jankus, F.B. Dias, A.P. Monkman, *Phys. Chem. Chem. Phys.,* 2014, **16,** 21543–21549.
65 B. Ries, H. Bassler, *Phys. Rev. B,* 1987, **35,** 2295–2302.
66 V.R. Nikitenko, D. Hertel, H. Bassler, H., *Chem. Phys. Lett., 2001,* **348,** 89–94.
67 M. Vissenberg, M.J.M DeJong, *Phys. Rev. Lett.,* 1996*,* **77,** 4820–4823.